Table 83. A summary of the hyperfine results for Ni_2MnGa [85J2].

Site	Probe	Method/parent	T [K]	H [kOe]
Ni	Ni	NMR	0	± 125
	^{99}Ru	TDPAC/^{99}Rh	293	– 110(10)
			77	185(10)
			0	188(11)
	^{111}Cd	TDPAC/^{111}Ag	293	202(10)
			0	310(10)
Mn	Mn	NMR	0	– 297
Ga	^{69}Ga/^{71}Ga	NMR	0	– 29
	^{119}Sn	ME	295	+ 15(5)
			4.2	38(3)
			0	38(3)
	^{111}Cd	TDPAC/^{111}In	333	93(3)
			293	– 160
			195	197(4)
			77	226(3)
			0	228(3)

Table 84. Normalised hyperfine fields at the non-magnetic sites Ni and Ga in Ni_2MnGa [85J2].

Site	Probe	A [kG]	H [kOe]	h [Oe/G]
Ni	Ni	2.4	± 125	± 52.1
	Ru	4.1	– 188	– 45.9
	Cd	7.2	– 310	– 43.1
Ga	Ga	6.2	– 29	– 4.68
	Sn	13	+ 38	+ 2.92
	Cd	7.2	– 228	– 31.7

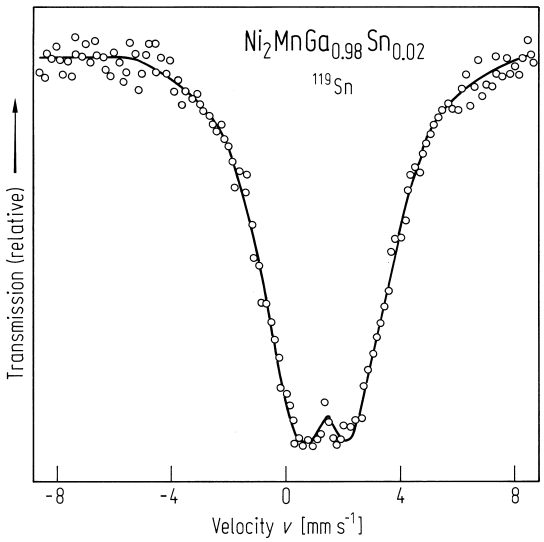

Fig. 389. ^{119}Sn Mössbauer effect spectra from Ni_2MnGa at 4.2 K (2 % of the Ga had been replaced by ^{119}Sn.) [85J2].

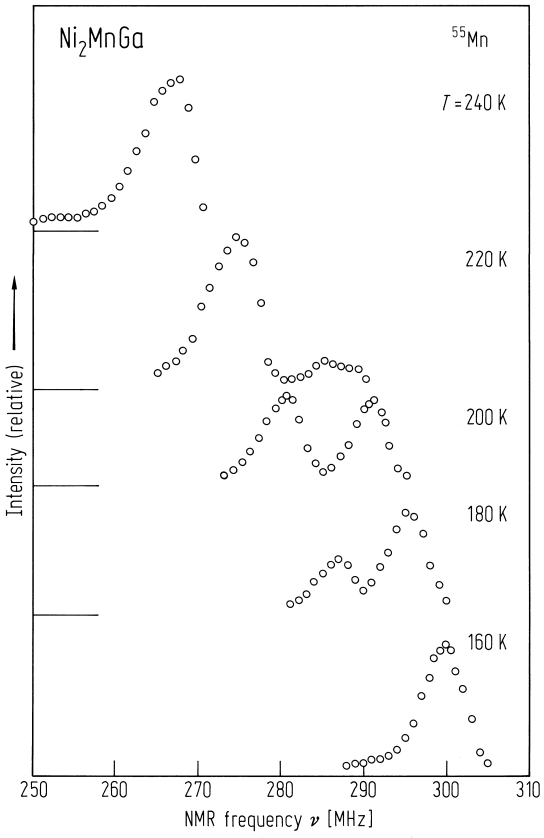

Fig. 388. The NMR spectra of ^{55}Mn for Ni_2MnGa from 160 to 240 K through the phase transition at T_t = 202 K [84W1]. The signal at 160 K is from the tetragonal state and at 240 K from the cubic state. Two lines are observed around T_t [92O1].

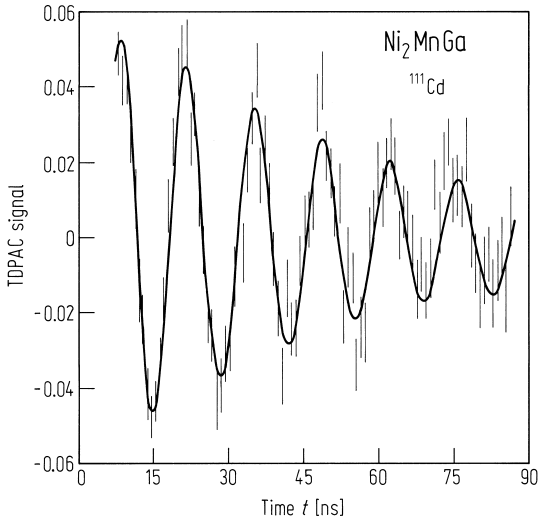

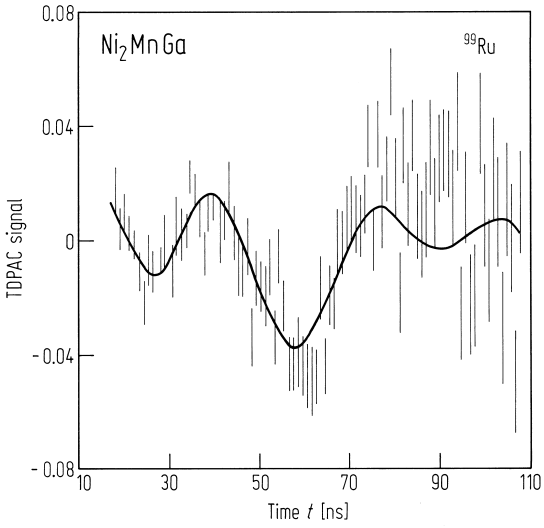

Fig. 390. ^{99}Ru TDPAC spectra for Ni_2MnGa obtained from the decay of ^{99}Rh on the Ni site at room temperature without external field [85J2].

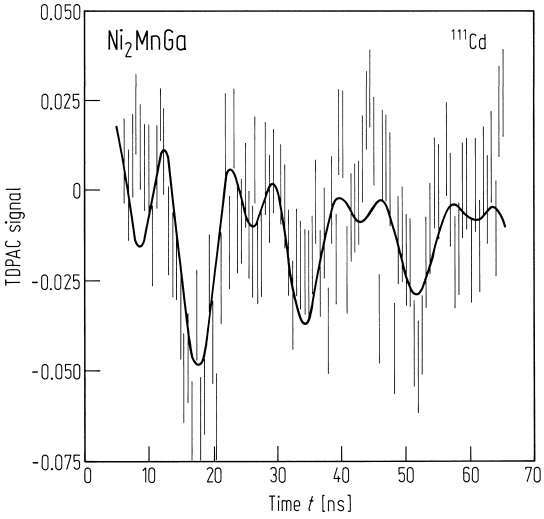

Fig. 392. Room temperature ^{111}Cd TDPAC spectra for Ni_2MnGa obtained from the decay of ^{111}Cd at the Ni site without an externally applied field [85J2].

Fig. 391. ^{111}Cd TDPAC spectra for Ni_2MnGa obtained from the decay of ^{111}In at the Ga site at room temperature and in an externally applied field [85J2].

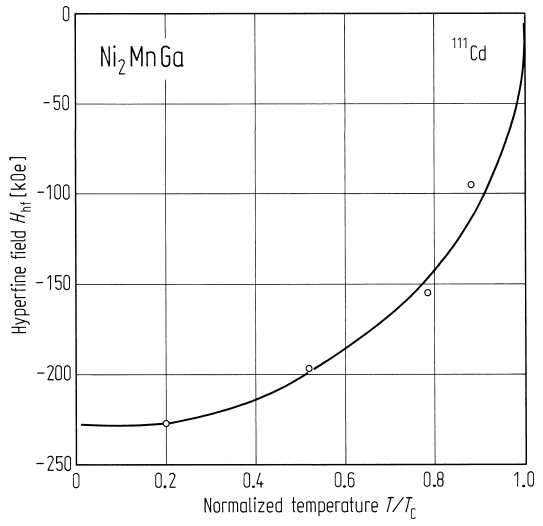

Fig. 393. Temperature dependence of the ^{111}Cd field at the Ga site in Ni_2MnGa. The solid curve is the Brillouin function for spin 5/2 [85J2]. The measurements did not reveal any anomaly at 202 K; Ni_2MnGa undergoes a martensitic phase transition at 202 K [85J2].

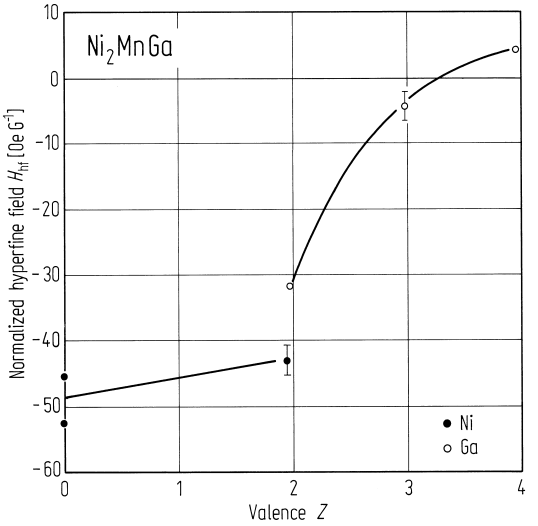

Fig. 394. Normalised hyperfine fields as a function of effective probe valence at Ni sites and Ga sites in Ni_2MnGa [85J2].

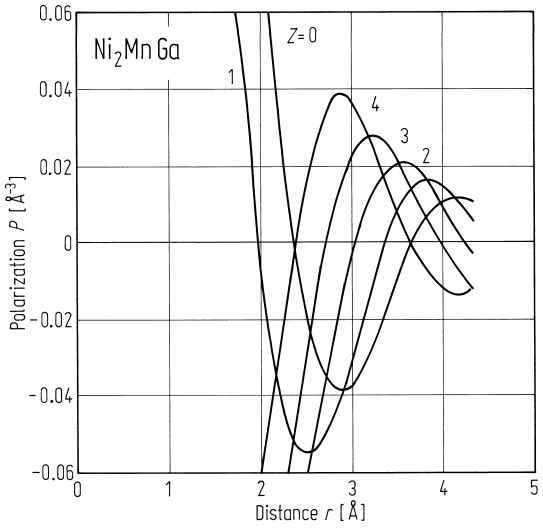

Fig. 395. Conduction electron polarisation per unit moment for different probe valences Z in Ni_2MnGa. The distances are measured from the magnetic Mn atom [85J2].

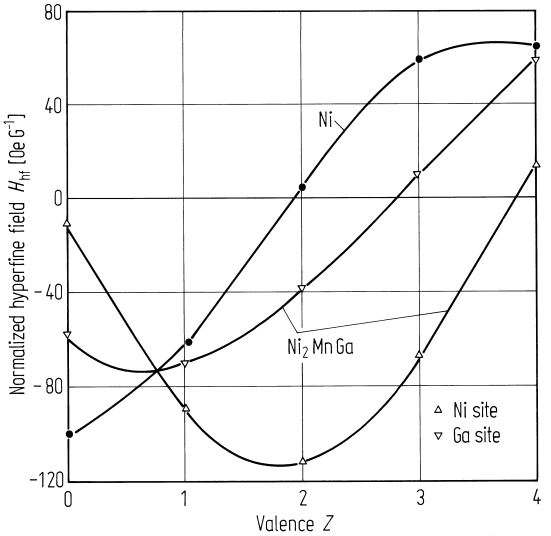

Fig. 396. Theoretical predictions for the normalised hyperfine field at Ni and Ga sites in Ni_2MnGa and Ni [85J2].

Summary of results

Table 85. A summary of hyperfine fields at T = 0 K in Heusler alloys [83J1].

X_2MnZ	a [Å]	p [μ_B]	H_X [kOe]	H_{Mn} [kOe]	H_Z [kOe]
Ni_2MnGa	5.825	4.17	Ni 125 Ru – 180 + 10 Cd (153)	Mn – 297	Ga – 29 Cd – 228 ± 3 Sn 16
Ni_2MnIn	6.068	4.4	Ni 141	Mn – 302	Mn – 386 Cd – 160 ± 1 In – 58.5 Sn 109
Ni_2MnSn	6.052	4.05	Ni – 127	Mn – 317	Mn + 253 Cd 181 ± 3 Sn + 87
Ni_2MnSb	6.000	3.27	Ni – 60	Mn – 285	Cd – 225 ± 3 Sn + 52 Sb + 293
Cu_2MnAl	5.949	2.96	Cu – 212	Mn – 214 Al + 75	Mn + 202 Al – 35.4 Cd 288 ± 7 Sn 50 ± 4
Cu_2MnIn	6.206	3.95	Cu – 200	Mn – 233	Cd – 217 ± 1 In – 93.2 Sn + 196
Cu_2MnSn	6.173	4.11	Cu – 175	Mn – 231	Cd 170 ± 3 Sn + 200 ± 10
Rh_2MnGe	6.030	4.62	Ru 196 ± 11 Cd (190)	Sn (10)	Cd – 203 ± 3 Sn 46.8 ± 1
Rh_2MnSn	6.252	3.10	Ru – 188 ± 3 Rh – 185	Mn 360	Cd – 190 ± 5 Sn + 21 Rh – 148
Rh_2MnPb	6.332	4.12	Rh 278	Mn 394	Cd – 144 ± 2 Sn + 24 ± 2 Pb (+) 53 Rh 206
Pd_2MnGe	6.174	3.2			Cd 264 ± 3
Pd_2MnSn	6.380	4.27	Pd – 255	Mn – 380 Cd + (80) In + 147 Sn + 270	Mn + 303 Cd – 205 ± 2 In – 162 Sn – 37.2
Pd_2MnSb	6.424	4.40	Pd – 88 Cd ≈ – 100	Mn – 330 Cd ≈ + 180	Cd – 232 ± 3 Cd ≈ – 240 Sn + 210 ± 5 Sb 579 Te 860 ± 5 I 507 ± 5

Table 86. A summary of hyperfine magnetic field data for X_2MnSn compounds with X = Co, Ni, Cu and Rh [85S1].

Alloy	T_C [K]	p [μ_B]	T [K]	ω_L [10^6 s^{-1}]	B [kG]
Co_2MnSn	829	5.08	77	289 ± 1	199 ± 1
			293	242 ± 3	167 ± 2
			473	200 ± 3	138 ± 2
Ni_2MnSn	344	4.05	77	269 ± 3	186 ± 2
			293	179 ± 2	124 ± 1
Cu_2MnSn	530	4.11	77	247 ± 1	171 ± 1
			293	195 ± 1	135 ± 1
Rh_2MnSn	420	3.1	77	199 ± 6	137 ± 4
			293	168 ± 2	116 ± 1
			373	68 ± 2	47 ± 1

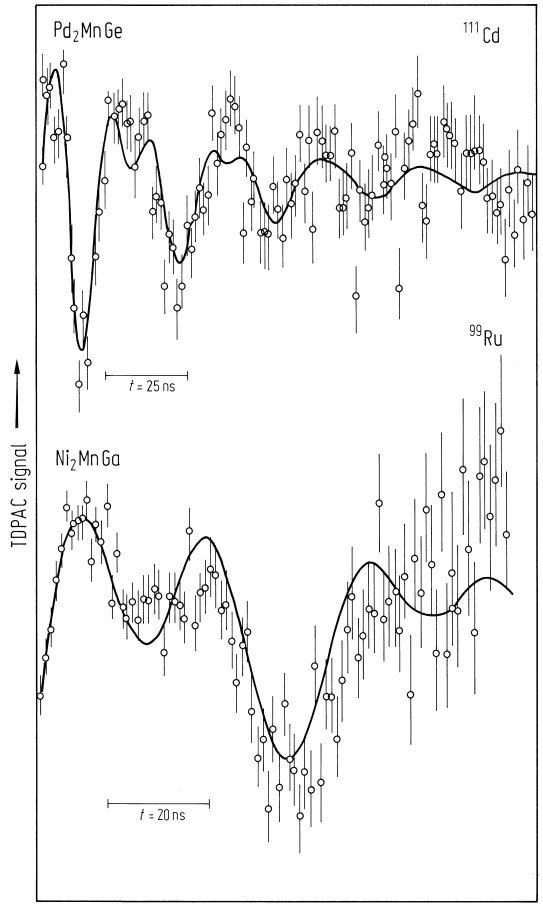

Fig. 397. TDPAC spectra of ^{111}Cd in Pd_2MnGe at 77 K and ^{99}Ru in Ni_2MnGa at 293 K [83J1].

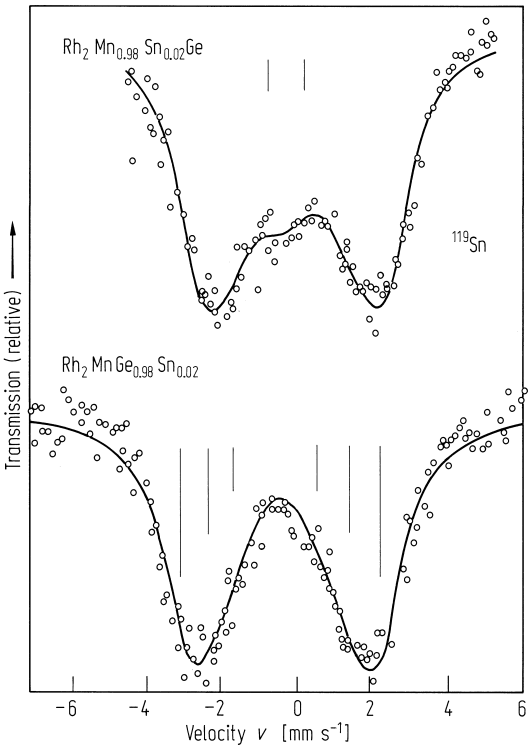

Fig. 398. Mössbauer spectra taken at 293 K for ^{119}Sn in $Rh_2Mn_{0.98}Sn_{0.02}Ge$ and $Rh_2MnGe_{0.98}Sn_{0.02}$ [83J1].

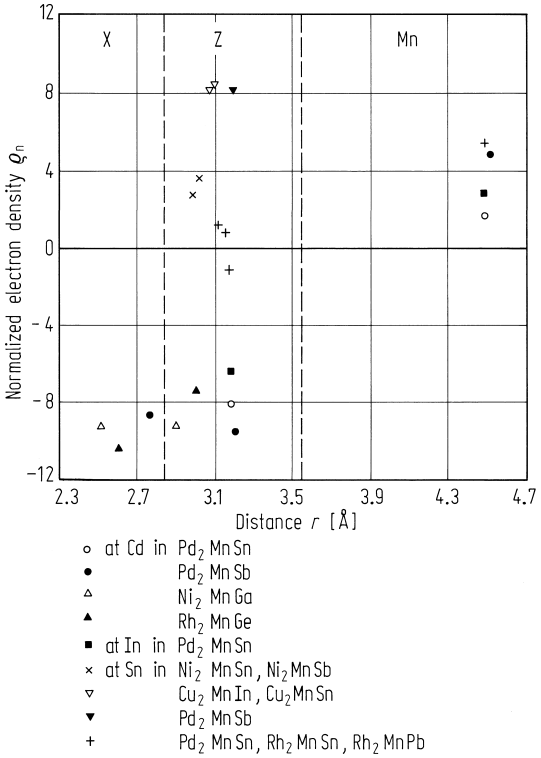

Fig. 399. Normalised polarised electron density vs. distance *r* to nearest Mn [83J1].

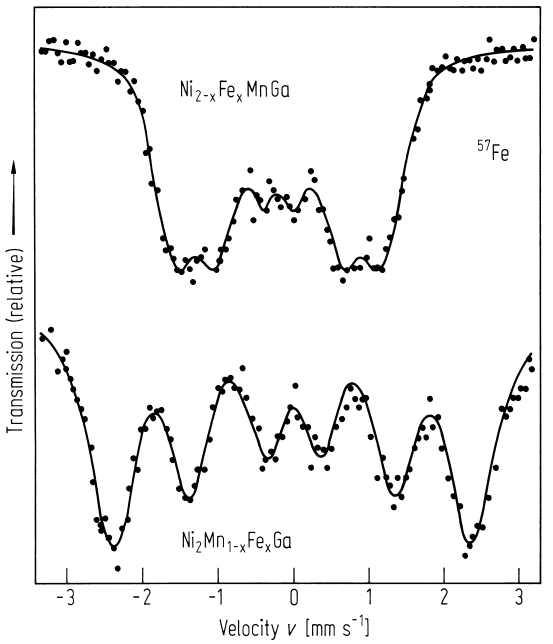

Fig. 401. Room-temperature Mössbauer spectra of ^{57}Fe in $Ni_{2-x}Fe_xMnGa$ and $Ni_2Mn_{1-x}Fe_xGa$ [87M1].

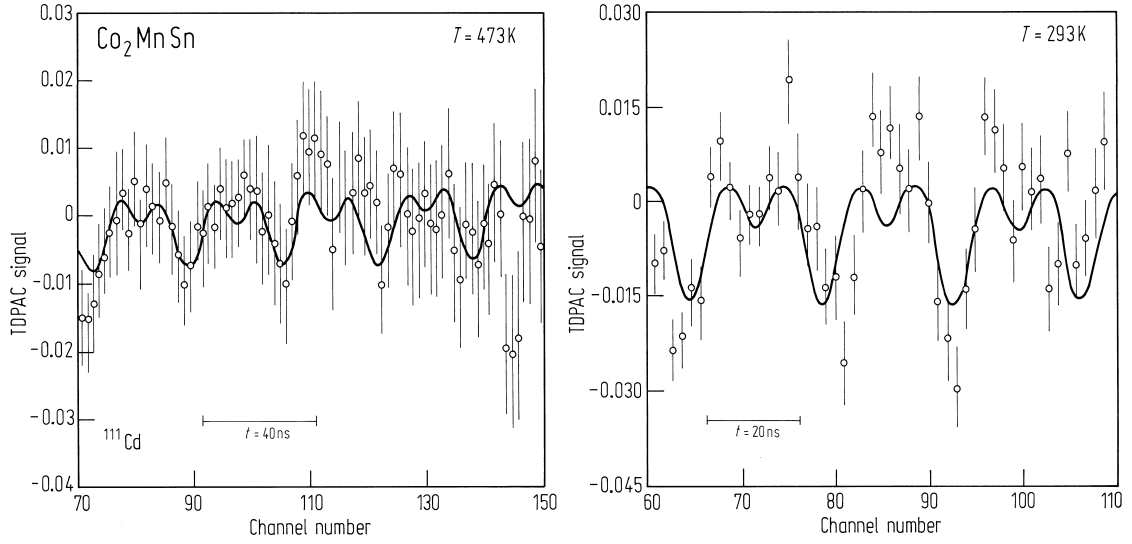

Fig. 400. TDPAC data for ^{111}Cd in Co_2MnSn [85S1].

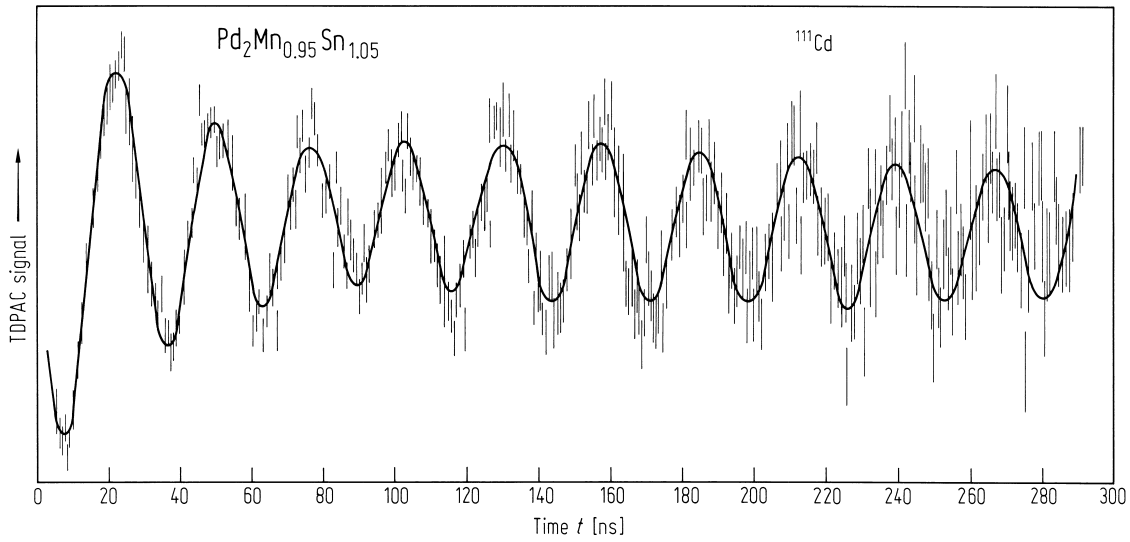

Fig. 402. Reduced time spectrum for ^{111}Cd in $Pd_2Mn_{0.95}Sn_{1.05}$ at 77 K [87M1].

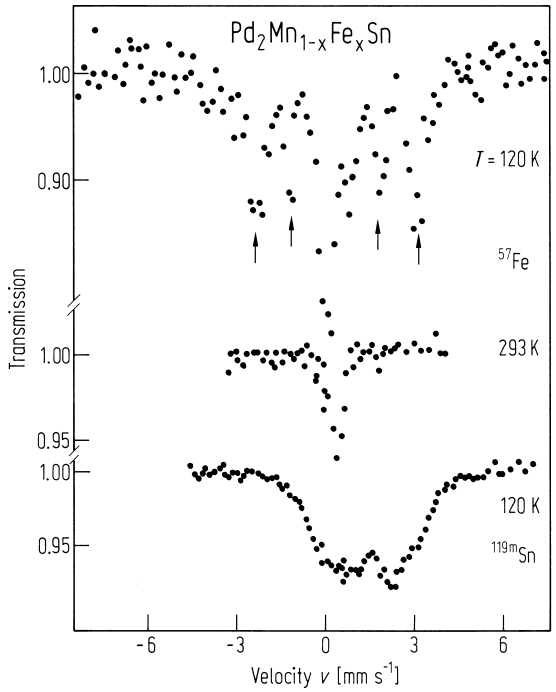

Fig. 403. Mössbauer spectra of ^{57}Fe in $Pd_2Mn_{1-x}Fe_xSn$ at 120 K and 293 K (both with $^{57}Co(Rh)$ source) and of ^{119}Sn at 120 K ($Ca^{119}SnO_3$) source [87M1].

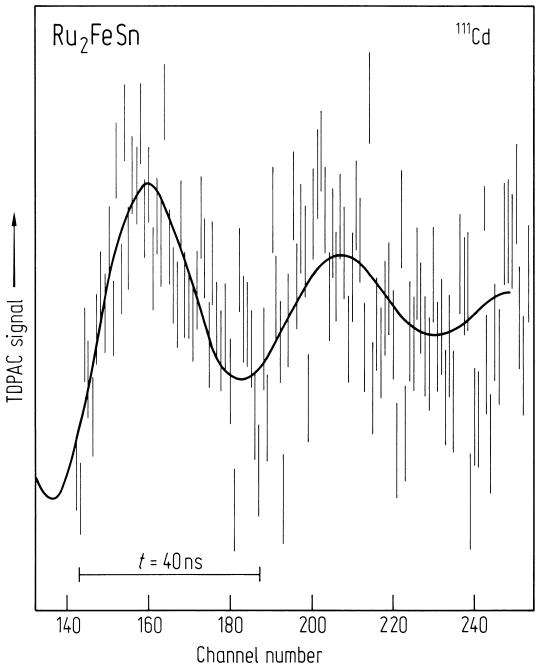

Fig. 404. Reduced time spectrum for ^{111}Cd in Ru_2FeSn at 293 K and in a field of 0.2 T [87M1].

Magnetic and mechanical induced anomalies

^{119}Sn Mössbauer spectra from Pd_2MnSn have revealed evidence of magnon-plasma and electron-magnon coupling. The effects of cold working which introduced dislocations and hence changes the atomic environment have also been investigated.

Table 87. Energy eigenvalues of the occupied core orbitals and electron density at the nuclear site of Sn in the ferro- and paramagnetic phases of Pd_2MnSn. The energy scale is given in Hartree atomic units (27.2 eV), and the electron density is in atomic units, with a_0 being the Bohr radius [83W2].

Orbital	Spin	Ferromagnetic energy	Paramagnetic energy
1s	↑	– 1026.23536	– 1026.26912
	↓	– 1026.30260	– 1026.26912
2s	↑	– 151.00142	– 151.03513
	↓	– 151.06857	– 151.03513
2p	↑	– 141.29825	– 141.33197
	↓	– 141.36543	– 141.33197
3s	↑	– 28.60459	– 28.63834
	↓	– 28.67178	– 28.63834
3p	↑	– 24.59650	– 24.63025
	↓	– 24.66369	– 24.63025
3d	↑	– 17.13591	– 17.16964
	↓	– 17.20308	– 17.16964
4s	↑	– 4.02763	– 4.06136
	↓	– 4.09473	– 4.06136
4p	↑	– 2.69369	– 2.72743
	↓	– 2.76080	– 2.72743
4d	↑	– 0.49066	– 0.52427
	↓	– 0.55751	– 0.52427
5s	↑	– 0.00662	– 0.01811
	↓	– 0.03267	– 0.01811
$n(0) = (a_0^{-3})$	↑	43739.44	43739.33
	↓	43739.34	43739.33

Table 88. The relative linewidths of NMR lines after slow cooling, $\Delta_1 = \Delta\omega_1/\omega_0$, and after cold work, $\Delta_2 = \Delta\omega_2/\omega_0$, and of the X-ray diffraction after slow cooling, $\delta_1 = \delta\theta_1/\theta_0$, and cold work $\delta_2 = \delta\theta_2/\theta_0$. ω_0 and $\Delta\omega$ are the NMR resonance frequencies and linewidth at half height respectively for the X (Pd, Ni, Cu), Y (Mn) and Z (Sn, Sb, In, Al) atoms. θ_0 and $\delta\theta$ are the diffraction angle and the angular width at half height of the (220) X-ray line. Pd_2MnIn is an antiferromagnet, so no NMR spectra were observable [83S1].

X_2YZ	Crystal structure	Δ_1 [10^3]			Δ_2 [10^3]			δ_1 [10^3]	δ_2 [10^3]
		X	Y	Z	X	Y	Z		
Pd_2MnSn	$L2_1$	6.8	0.5	52.0	11.4	2.5		7.0	16.0
Pd_2MnSb	$L2_1$		2.8	5.5		5.0	16.0	4.5	17.7
Pd_2MnIn	$\approx L2_1$							8.2	20.3
Ni_2MnIn	$\approx L2_1$		≈ 3.0	≈ 65.0		≈ 6.0	≈ 65.0	5.2	16.0
Cu_2MnAl	$L2_1$	4.0	4.0	10.0	4.6	4.5	26.0	7.0	10.2
Cu_2MnIn	$L2_1$	2.3	1.6	17.6	27.3	20.7	82.4	7.8	18.0
Ni_2MnSb	$C1_b$		0.7	2.5		0.7	2.5	6.0	6.0

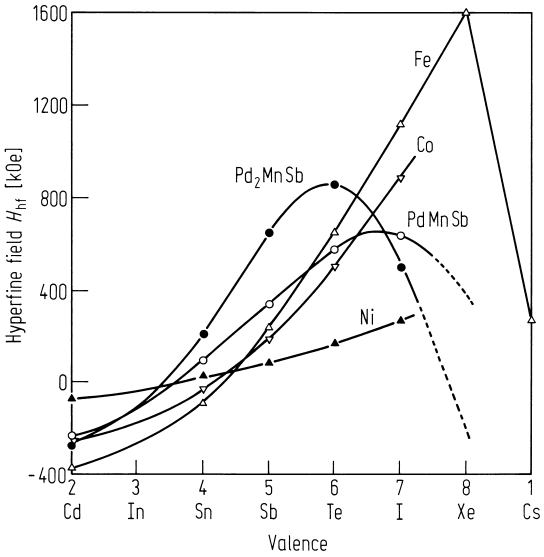

Fig. 405. Trends of measured magnetic hyperfine fields at 5 sp impurity atoms in Pd_2MnSb, PdMnSb, Fe, Co and Ni hosts [83W2].

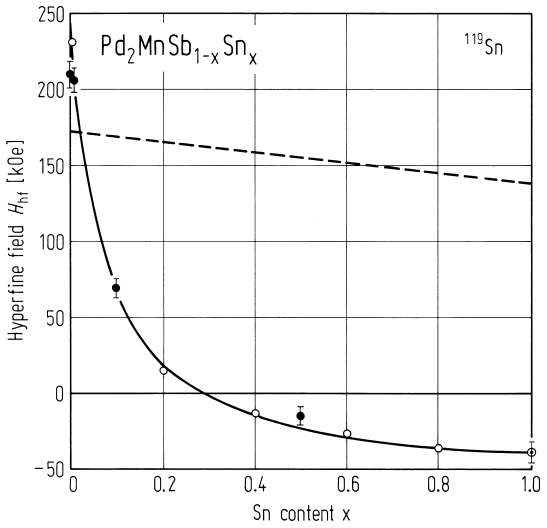

Fig. 406. ^{119}Sn hyperfine fields in $Pd_2MnSb_{1-x}Sn_x$ observed as a function of Sn content x. The broken line gives the prediction of these fields based on the Jena-Geldart Model [83W2].

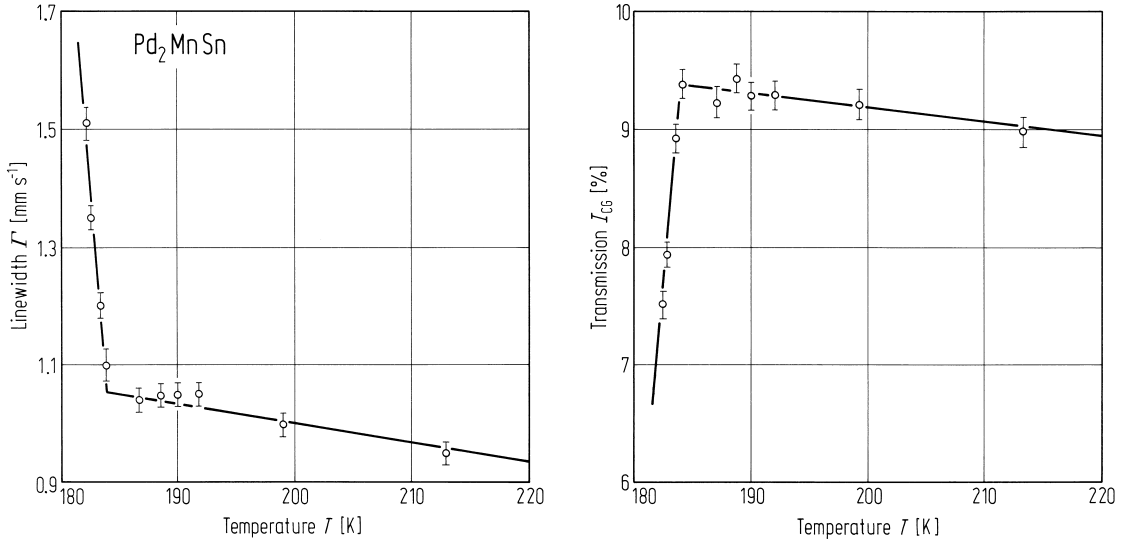

Fig. 409. Temperature dependence of the linewidth Γ and centroid velocity transmission I_{CG} near the Curie temperature in Pd_2MnSn [83W2].

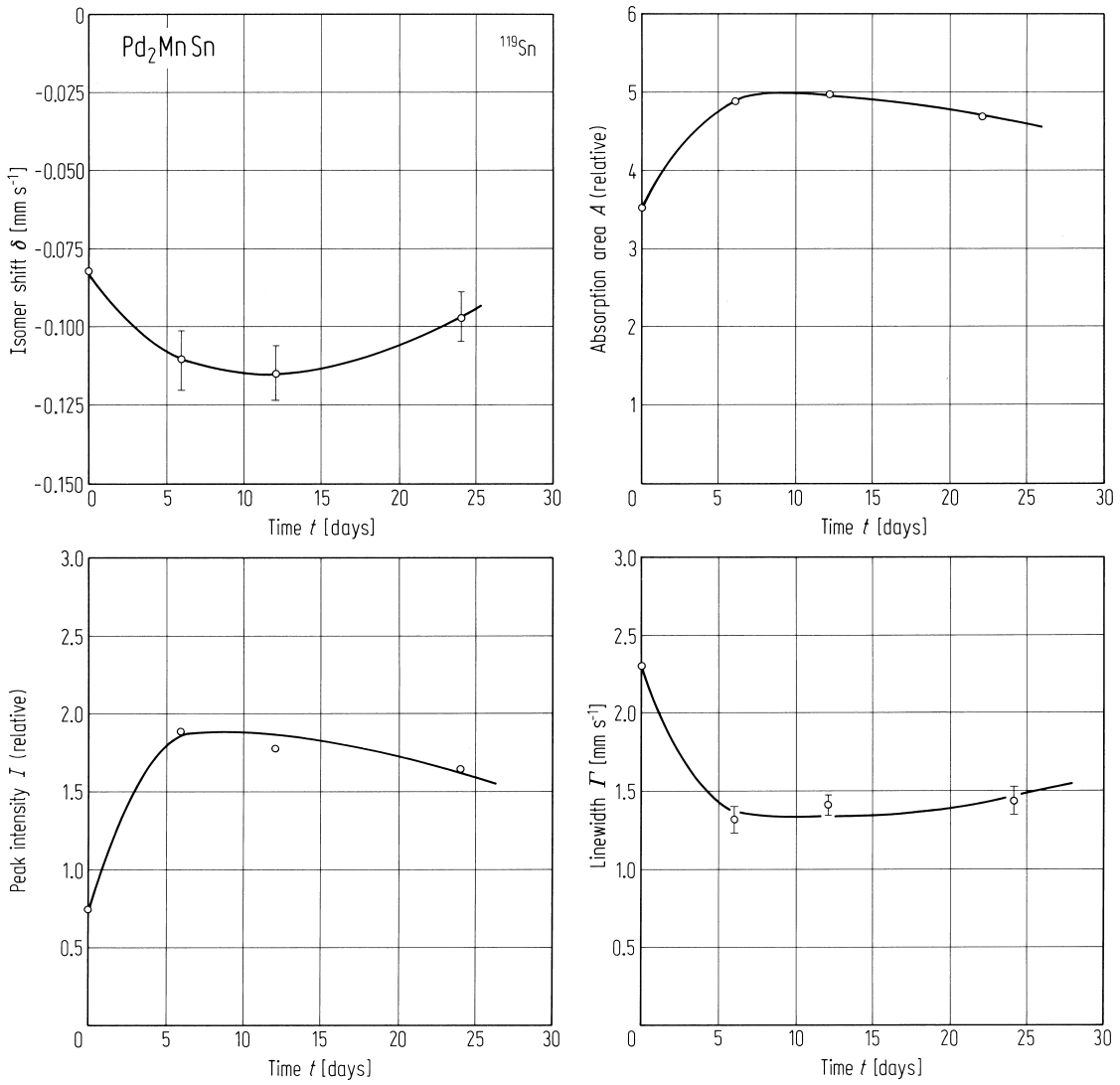

Fig. 407. Annealing effects shown in the Mössbauer spectra of ^{119}Sn in Pd_2MnSn at 78 K; δ denotes the isomer shift of Sn in Pd_2MnSn relative to ^{119}Sn in vanadium. A is the resonant absorption area, I is the peak intensity and Γ is the observed linewidth [83W2].

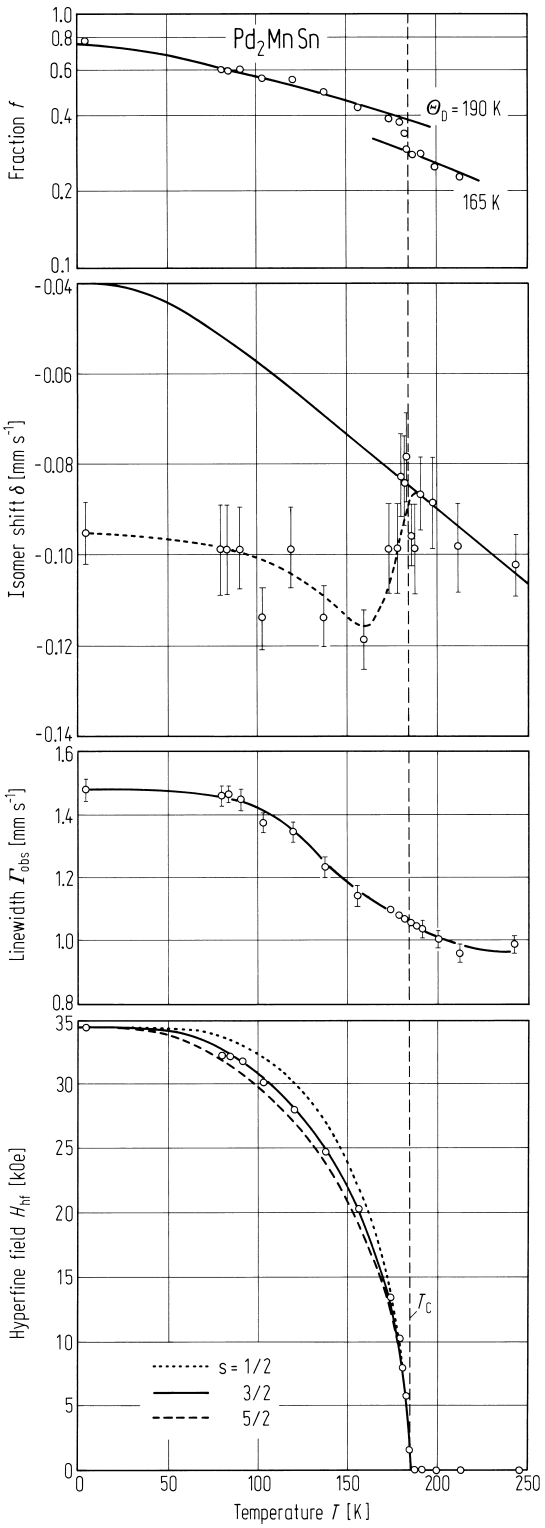

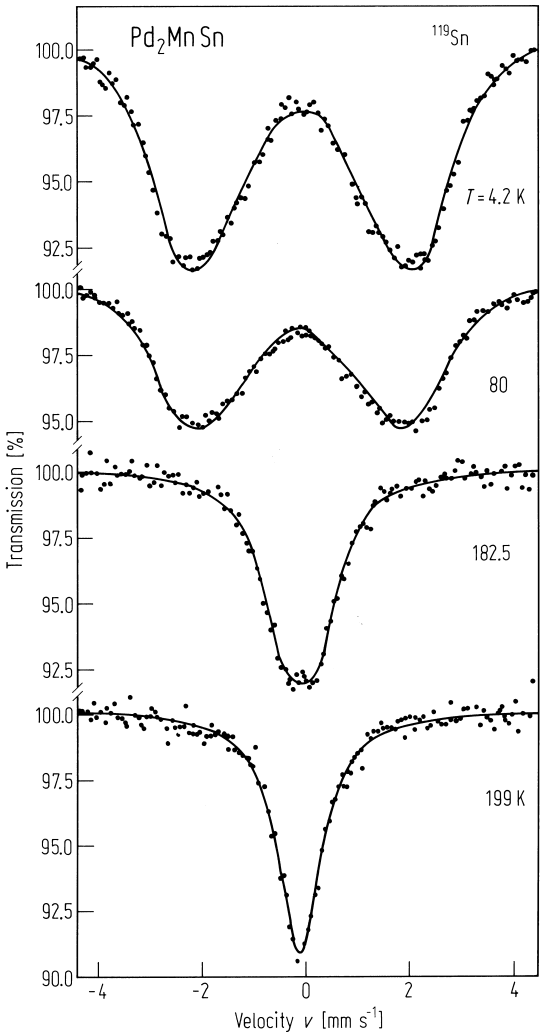

Fig. 408. Mössbauer spectrum of Pd_2MnSn at the temperatures indicated [83W2].

Fig. 410. Temperature variation of the recoil-free fraction f, the isomer shift δ, the observed linewidth Γ_{obs} and the internal magnetic field H_{hf} at the Sn site in Pd_2MnSn [83W2].

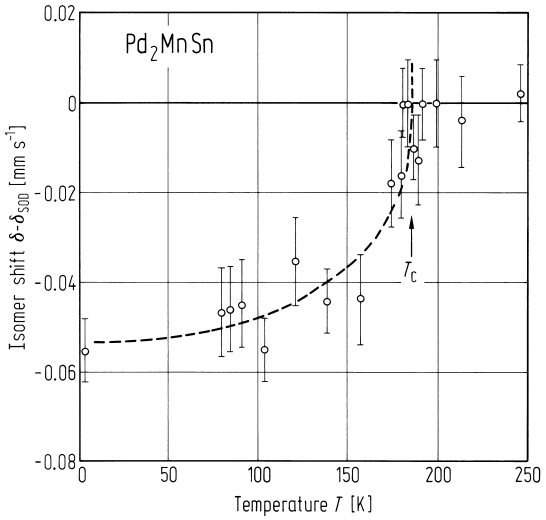

Fig. 411. Temperature variation of the chemically-induced ^{119}Sn isomer shift for $T < T_C$ in Pd_2MnSn [83W2].

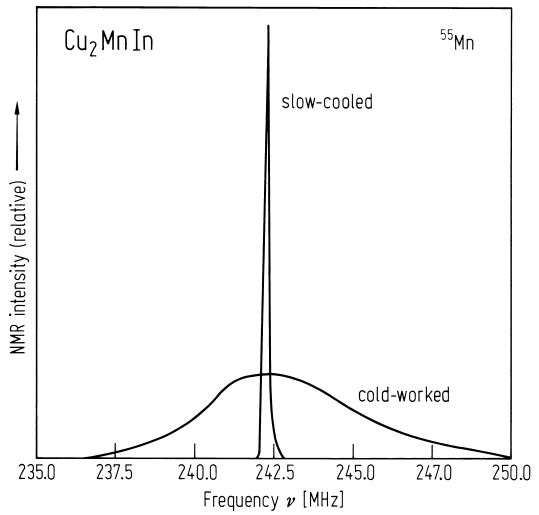

Fig. 412. Mn NMR line of Cu_2MnIn as slow-cooled and as cold-worked [83S1].

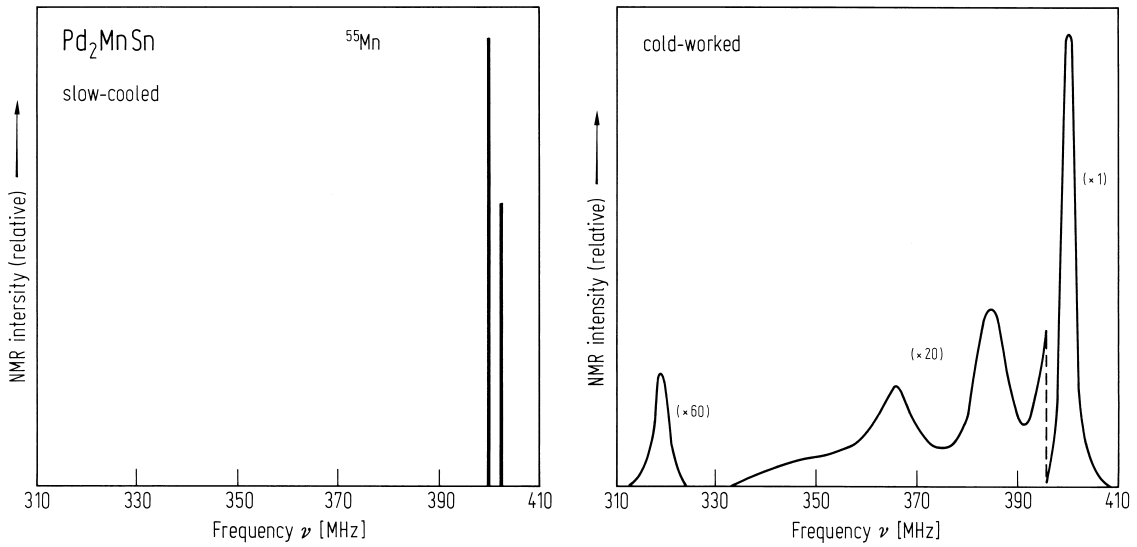

Fig. 413. Mn NMR spectrum of Pd_2MnSn as slow-cooled and as cold-worked [83S1].

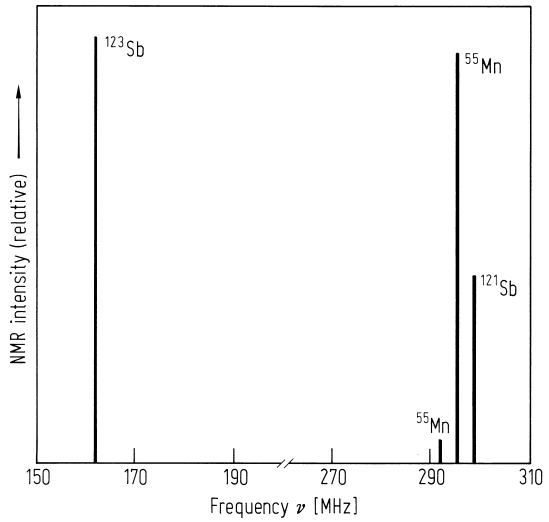

Fig. 414. Mn and Sb NMR lines of NiMnSb as slow cooled or as cold worked [83S1].

X_2YZ X = 3d, Y = 3d

X = 8A: Co
Y = 4A: Ti; 5A: V; 6A: Cr; 7A: Mn; 8A: Fe
Z = 3B: Al, Ga; 4B: Si, Ge, Sn

Hyperfine fields have been calculated by the KKR method with the aim of establishing the effect of the Z atom on the magnetic properties. The hyperfine field at the Co site changes drastically with Y from a positive value for Ti to a negative value for Fe. The change occurs mainly in the contribution to the hyperfine field from the valence electrons which are sensitive to the neighbouring magnetic moments. The calculated hyperfine fields on the Co and Mn sites are smaller than the experimental values, although the trend as a function of Z agrees.

Table 89. Calculated magnetic moments of constituent atoms in Co_2TZ alloys and those per molecule. The measured values are given in brackets [91I1].

Co_2YZ	p_S [μ_B/f.u.]	p_{Co} [μ_B]	p_Y [μ_B]	p_Z [μ_B]
Co_2TiGa	0.97 (0.75)	0.59 (0.40)	– 0.19	– 0.01
Co_2VGa	1.95 (1.92)	0.93 (1.05)	0.09	– 0.01
Co_2CrGa	3.01 (2.36)	0.96 (0.8)	1.14 (1.1)	– 0.05
Co_2MnGa	4.21 (4.05)	0.72 (0.52)	2.87 (3.01)	– 0.10
Co_2FeGa	5.02 (5.13)	1.16 (1.0)	2.77 (3.10)	– 0.06
Co_2VAl	1.97 (1.95)	0.94 (0.92)	0.11	– 0.03
Co_2MnAl	4.10 (4.04)	0.72 (0.5)	2.80 (3.01)	– 0.13
Co_2FeAl	4.98 (4.96)	1.16	2.76	– 0.10

Table 90. Calculated hyperfine fields of constituent atoms in Co_2TZ in kOe. Experimental values are listed in the column H_{exp}. The last column shows the difference of s electrons between majority and minority spins. H_{cal} is a calculated value and H_{val} and H_{core} are the contributions to H_{cal} from inner core s electrons and valence s electrons respectively [91I1].

		H_{core} [kOe]	H_{val} [kOe]	H_{cal} [kOe]	H_{exp} [kOe]	n_s
Co_2TiGa	Co	– 65.61	100.57	34.96	12.2	0.017
	Ti	20.35	– 68.61	– 48.26		– 0.013
	Ga	0.00	– 4.49	– 4.49		
Co_2VGa	Co	– 90.79	148.04	57.25	14.3	0.025
	V	– 6.63	– 77.58	– 84.21	– 73	– 0.014
	Ga	0.00	– 27.82	– 27.82		
Co_2CrGa	Co	– 100.33	88.94	– 11.39	– 35.8	0.015
	Cr	– 91.80	– 47.61	– 139.41		– 0.010
	Ga	1.06	– 64.67	– 63.61		
Co_2MnGa	Co	– 79.50	– 55.46	– 134.96	– 171.8	– 0.011
	Mn	– 289.12	77.61	– 211.51	– 280.0	0.010
	Ga	2.12	– 26.19	– 24.07		
Co_2FeGa	Co	– 119.73	– 10.83	– 130.56	– 182.0	– 0.004
	Fe	– 276.82	47.84	– 228.98		0.003
	Ga	1.59	25.77	27.36		
Co_2VAl	Co	– 90.87	152.78	57.91	18.0	0.026
	V	– 9.38	– 70.64	– 80.00	– 63.4	– 0.014
	Al	0.69	– 16.61	– 15.92	– 7	
Co_2MnAl	Co	– 81.78	– 64.46	– 146.24	– 175.1	– 0.013
	Mn	– 284.77	75.24	– 209.53	– 280.5	0.009
	Al	2.12	– 26.19	– 24.07		
Co_2FeAl	Co	– 121.05	– 7.28	– 128.33	– 194.0	– 0.004
	Fe	– 276.45	68.92	– 207.53		0.007
	Al	2.88	– 9.70	– 6.82		

Table 91. A summary of hyperfine field parameters calculated using the KKR method. H_{core} and H_{val} are the contributions to the hyperfine fields from the core and valence s electrons. $H_{cal} = H_{core} + H_{val}$. H_{exp} are experimental values taken from (a) [78L1], (b) [85Y1], (c) [87K2] and (d) [89K1]. The last column shows the difference of s electrons between majority and minority spin [90F2].

		H_{core} [kOe]	H_{val} [kOe]	H_{cal} [kOe]	H_{exp} [kOe]	n_s
Co_2MnAl	Co	– 77.3	– 61.4	– 138.6	– 177 [(d)] – 175.1 [(b)]	– 0.008
	Mn	– 290.8	84.3	– 206.5	– 280.5 [(d)]	0.010
	Al	3.5	– 28.0	– 24.5		– 0.009

		H_{core} [kOe]	H_{val} [kOe]	H_{cal} [kOe]	H_{exp} [kOe]	n_s
Co_2MnGa	Co	– 73.3	– 54.9	– 128.1	– 171.8 [c] – 173 [a]	– 0.008
	Mn	– 292.6	87.2	– 205.5	– 280.0 [c] – 280 [a]	0.010
	Ga	1.6	– 26.6	– 25.0		– 0.005
Co_2MnSi	Co	– 101.2	30.3	– 70.9	– 145.0 [c] – 146 [a]	0.004
	Mn	– 305.2	83.9	– 221.3	– 335.9 [c] – 337 [a]	0.010
	Si	3.3	9.8	13.1		– 0.000
Co_2MnGe	Co	– 99.6	23.5	– 76.1	– 140.2 [c] – 141 [a]	0.003
	Mn	– 311.1	84.6	– 226.5	– 339.4 [c] – 339 [a]	0.010
	Ge	2.1	65.6	67.7		0.003
Co_2MnSn	Co	– 96.9	– 4.8	– 101.7	– 156.0 [c] – 155 [a]	– 0.001
	Mn	– 324.6	103.3	– 221.3	– 344.1 [c] – 352 [a]	0.013
	Sn	2.7	– 41.7	– 39.1		– 0.004

Table 92. Calculated moment in Bohr magnetons for different sites calculated using the LSD method, [84I2] compared with experimental values and the calculation of Kübler [83K4].

X_2YZ		p [μ_B]	p_X [μ_B]	p_Y [μ_B]	p_Z [μ_B]
Cu_2MnAl	calc	3.20	– 0.01	3.28	– 0.08
	exp	3.60	$0 < m < 0.1$		
	Kübler	3.38		3.36	
Ni_2MnSn	calc	4.03	0.21	3.62	– 0.05
	exp	4.05			$0 < m < 0.1$
	Kübler	3.75		3.39	
Pd_2MnSn	cal	4.05	0.04	4.00	– 0.07
	exp	4.23 ± 0.1	0.1 ± 0.05	4.33	$-0.1 < m < 0$
	Kübler	3.86		3.78	
Pd_2MnSb	calc	4.09	0.04	4.02	– 0.06
	exp	4.40			
	Kübler	4.0		3.82	
Co_2MnSn	calc	5.02	0.91	3.30	– 0.06
	exp	5.08 ± 0.05	0.75 ± 0.08	3.58 ± 0.16	
	Kübler	5.02		3.13	

X_2YZ		p [μ_B]	p_X [μ_B]	p_Y [μ_B]	p_Z [μ_B]
Co_2TiSn	calc	1.32	0.72	0.09	0.0
	exp	193 ± 0.07	1.03 ± 0.1		
Co_2TiAl	calc	0.26	0.16	0.05	0.0
	exp	0.71	0.35 ± 0.1		
Mn_2VAl	calc	1.98	1.44	– 0.85	– 0.02
	exp	1.9	1.2	– 0.7	

Table 93. Hyperfine fields for the constituent atoms in the Heusler alloys. The experimental values and the spin polarisations of the valence s-electrons (Δn_s) are also listed [84I2].

X_2YZ		H_X [kOe]	H_Y [kOe]	H_Z [kOe]
Cu_2MnAl	calc	– 208	– 66	– 27
	exp	– 212	– 213	– 35
	Δn_s	– 0.28	0.036	– 0.011
Ni_2MnSn	calc	– 118	– 174	70
	exp	– 128	– 315	95
	Δn_s	– 0.012	0.027	0.002
Pd_2MnSn	calc	– 143	– 189	– 17
	exp	– 255	– 380	– 38
	Δn_s	– 0.011	0.034	– 0.003
Pd_2MnSb	calc	– 66	– 173	211
	exp	– 88	– 328	625
	Δn_s	– 0.005	0.037	0.009
Co_2MnSn	calc	– 105	– 222	– 17
	exp	– 155	– 352	105
	Δn_s	– 0.002	0.012	– 0.003
Co_2TiSn	calc	49	– 49	– 3
	exp	22		82
	Δn_s	0.018	– 0.008	– 0.001
Co_2TiAl	calc	41	– 11	– 3
	exp	17	– 24	– 2
	Δn_s	0.017	– 0.008	– 0.010
Mn_2VAl	calc	– 78	– 66	– 18
	exp	– 99	– 64	– 25
	Δn_s	0.016	– 0.018	– 0.005

Table 94. Hyperfine fields for Mn and Co in Heusler alloys. χ_{core} is χ associated with the core s-electrons. H_{core} and H_{val} are the contributions to the hyperfine fields arising from the core and valence s-electrons. H' is the hyperfine field when χ_{core} is – 3.1 and – 2.5 for Mn and Co in the Heusler alloys. The calculated fields H and H' are compared with the experimental fields H_{exp} [84I2].

		χ_{core} [kOe]	H_{core} [kOe]	H_{val} [kOe]	H [kOe]	H' [kOe]	H_{exp} [kOe]
Mn in	Cu_2MnAl	– 2.36	– 326	260	– 66	– 169	– 213
	Ni_2MnSn	– 2.37	– 362	189	– 174	– 285	– 315
	Pd_2MnSn	– 2.40	– 405	217	– 189	– 306	– 380
	Pd_2MnSb	– 2.36	– 400	226	– 174	– 300	– 328
	Co_2MnSn	– 2.28	– 318	96	– 222	– 336	– 352
	Mn_2VAl	– 2.11	– 128	50	– 78	– 138	– 99
Co in	Co_2MnSn	– 2.41	– 92	– 13	– 105	– 109	– 151
	Co_2TiSn	– 2.32	– 71	120	49	44	23
	Co_2TiAl	– 2.38	– 16	57	41	40	17

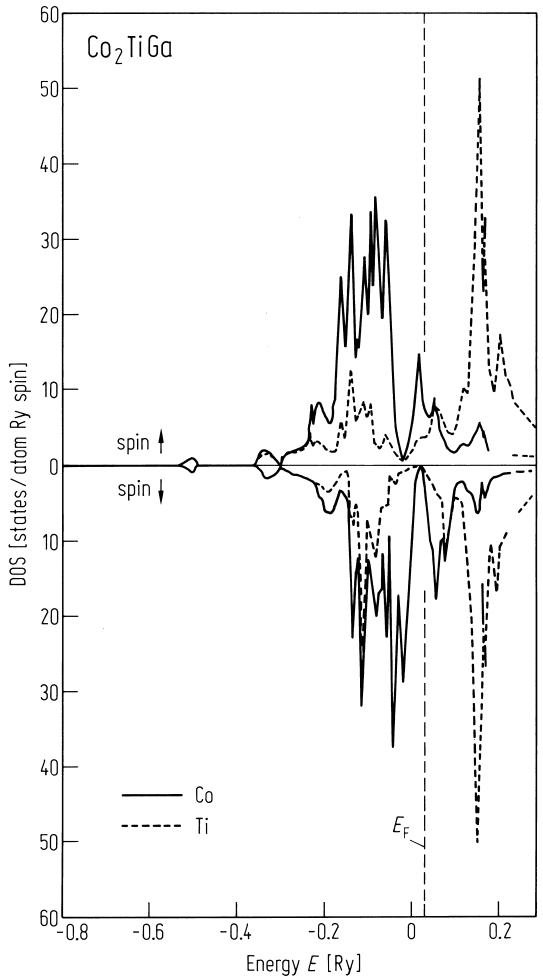

Fig. 415. DOS curves of d bands of Co and Ti atoms in Co_2TiGa. The full and broken curves show the DOS of Co and Ti atoms respectively and the DOS curves for up-spin electrons are shown in the upper part and those for down-spin electrons are shown in the lower part. The Fermi level is indicated by the vertical broken line [91I1].